Formation of Metal in GRO 95551 and Comparison to Ordinary Chondrites

ANDREW J. CAMPBELL* AND MUNIR HUMAYUN

Department of the Geophysical Sciences,

The University of Chicago, Chicago, Illinois 60637 USA

*email: a-campbell@uchicago.edu

ph: (773) 834-1523, fax: (773) 702-9505

Submitted to *Geochim. Cosmochim. Acta*: August 1, 2002

Revised: November 19, 2002

Accepted: December 9, 2002

Abstract–Siderophile element abundances in individual metal grains in the ungrouped chondrite GRO 95551 and in the ordinary chondrites Tieschitz H3.6, Soko-Banja LL4, and Allegan H5 were measured using laser ablation inductively-coupled plasma mass spectrometry. Matrix metal in GRO 95551 falls into two distinct compositional groups, a high-Ni group with 7.2 ± 0.4 wt% Ni and a low-Ni group with 3.7 ± 0.1 wt% Ni, indicating that kamacite/taenite equilibration at ~1020 K was followed by rapid cooling. The nonrefractory siderophile elements P, Co, Cu, Ga, Ge, As, Pd, and Au also partition between the high-Ni and low-Ni metal in a manner consistent with kamacite/taenite fractionation, but the refractory siderophiles Ru, Re, Os, Ir, and Pt show correlated variations that are unrelated to kamacite/taenite partitioning, and indicate that variations in refractory components of the metal were not completely erased during equilibration at ~1020 K. The Ni-normalized bulk metal composition of GRO 95551 is refractory-depleted and volatile-rich relative to Bencubbin and related metal-rich chondrites, but bears strong similarities to equilibrated ordinary chondrite metal. GRO 95551 represents a new chondrite type with chemical affinity to the ordinary chondrites. Individual metal grains in unequlibrated ordinary chondrites also have correlated variations in refractory siderophile contents that cannot be produced by redox processes alone; these variations span 3 orders of magnitude and diminish with increasing metamorphic grade of the ordinary chondrites.

1. INTRODUCTION

Iron-nickel metal is an important phase in chondrites, since it constitutes almost a third by mass of the condensable material in the inner solar nebula, and hosts the siderophile elements. However, most of the metal observed in ordinary chondrites (and presumably in enstatite chondrites) has been metamorphically re-equilibrated with its silicate matrix (Humayun and Campbell, 2002), and metal exhibiting chondritic Co/Ni ratios is rare in most carbonaceous chondrites (Grossman and Olsen, 1974) since it is destroyed by oxidation and hydrothermal alteration. Thus, the presence of a group of metal-rich chondrites exhibiting metal with chondritic Co/Ni ratios is of considerable cosmochemical significance; these include the CB (Bencubbin-like) chondrites, the CH (ALH 85085-like) chondrites, and the CR (Renazzo-like) chondrites (Weisberg et al., 1993, 2001). Many of these chondrites are new finds from Antarctica or the North African desert, and the metal in these meteorites is considered to provide astrophysical and cosmochemical clues to nebular processes (e.g., Newsom and Drake, 1979; Meibom et al., 2000).

Grosvenor Mountains (GRO) 95551 is a metal-rich chondrite that shares many of the unusual petrographic features that are found in the CB meteorites (Mason, 1997; Weisberg et al., 2001). Siderophile element data from metal clasts in Bencubbin and related meteorites have revealed an origin by volatilization or condensation from gas enriched in metal relative to solar gas, but which does not appear to reflect equilibrium with the solar nebula (Campbell et al., 2002). In contrast, individual zoned grains in some metal-enriched chondrites (e.g., QUE94411, HH237) have been shown to be consistent with condensation in a rapidly cooling gas of approximately solar composition (Weisberg et al., 1999; Meibom et al., 1999; Campbell et al., 2000, 2001; Petaev et al., 2001; Campbell and Humayun, 2002a). However, despite the noted textural similarities to CB chondrites, the

oxygen isotope composition of GRO 95551 is very different from Bencubbin and close to that of the ordinary chondrites (Weisberg et al., 2001).

Ordinary chondrites are the most common class of meteorites, and an understanding of their formation and evolution is crucial for interpretation of the early solar system in which they formed. The ordinary chondrites are further subdivided primarily in two ways: first, by their metal content, and second by the degree of metamorphism they experienced on their parent body subsequent to accretion. The metal phases in ordinary chondrites are expected to hold, in their siderophile element concentrations, a record of the processes associated with these subdivisions, and perhaps also of the pre-accretionary history of the metal. In particular, there has been debate surrounding the relationship between metal and chondrule formation. Some propose that metal/silicate and refractory/volatile fractionations occurred prior to chondrule formation, and that variations in chondrule composition are primarily the product of differences in chondrule precursor material (e.g., Grossman and Wasson, 1983, 1985; Jones, 1994). Others contend that chondrite metal was primarily produced by reduction of silicate melt during chondrule formation (Zanda et al., 1994; Connolly et al., 1994, 2001; Lauretta et al., 2001). Recent work on metal in the CR2 chondrites implicates recondensation of volatilized metal as another important process (Connolly et al., 2001; Humayun et al., 2002).

To extend our understanding of the formation of these meteorites, to determine whether metal and other phases in GRO 95551 have a nebular origin, and to investigate a possible link to the ordinary chondrites, we have measured the distribution of siderophile elements in metal in GRO 95551 and in the ordinary chondrites Allegan (H5), Soko-Banja (LL4), and Tieschitz (H3.6). Preliminary results of this study were reported by Campbell and Humayun (2002b).

2. EXPERIMENTAL

Polished thin section GRO 95551,12 was obtained from the United States Antarctic Meteorite Collection. Sample L3443 of Tieschitz (H3.6) was obtained from the Naturhistorisches Museum, Vienna. Samples Me 319 of Soko-Banja (LL4) and Me 1432 of Allegan (H5) were provided by the Field Museum of Natural History. The sections were examined optically and studied using a JEOL 5800LV scanning electron microscope (SEM) with an Oxford Link/ISIS EDX system. Point-counting on the SEM images was used to estimate the volume fraction of silicate, metal, and sulfide in GRO 95551. Compositions of each phase were measured by EDX, and locations were selected for trace siderophile element analysis by LA-ICP-MS.

The laser ablation system utilized a CETAC LSX-200 laser ablation peripheral with a Finnigan MAT Element ICP mass spectrometer (Campbell and Humayun, 1999a,b; Campbell et al., 2002, 2003). Experimental conditions for each analysis varied according to the size of the target grain and the elements to be analyzed. As many as 21 siderophile elements (plus Mg, Si and S to identify potential beam overlaps on silicate or sulfide phases) were determined by monitoring the isotopes ^{25}Mg, ^{29}Si, ^{31}P, ^{34}S, ^{51}V, ^{53}Cr, ^{57}Fe, ^{59}Co, ^{60}Ni, ^{63}Cu, ^{69}Ga, ^{74}Ge, ^{75}As, ^{95}Mo, ^{101}Ru, ^{105}Pd, ^{118}Sn, ^{121}Sb, ^{182}W, ^{185}Re, ^{192}Os, ^{193}Ir, ^{195}Pt, and ^{197}Au during some or all of the measurements; frequently a grain was analyzed twice, with different sets of siderophile elements measured in each analysis. Each analyzed point was ablated by 20-50 laser pulses at 10 Hz; the laser-ablated pits produced were 25-160 μm in diameter and approximately 10-25 μm deep. The mass spectrometer was swept repeatedly over the intended mass range while the ablated material was carried by Ar gas from the sample chamber to the mass spectrometer. The signal from the transient laser ablation pulse was integrated over a period of 20-25 s; this was sufficient time for the pulse to reach a peak intensity and then decay almost to background levels. Instrumental sensitivity factors for each isotope were determined by measuring signal intensity from the

group IVB iron meteorite Hoba, the group IIA iron meteorite Filomena, and the NIST reference steel SRM 1263a, which have known concentrations of the elements of interest (Campbell and Humayun, 1999b; Campbell et al., 2002).

Uncertainties reflect contributions from counting statistics as well as an instrumental error that is largely due to the transience of the signal. The counting errors incorporate both the measured counts and the counts in the blank measurement. The instrumental error was calculated from repeat measurements of the standards, by stripping away the counting errors from the standard deviations. This is a conservative estimate of the instrumental error because it assumes homogeneity in the standards, which are known to have fine scale heterogeneities. Instrumental errors (1σ) were assigned as 3%; this is the average value from several different calibrations.

3. RESULTS

The section GRO 95551,12 is approximately 8 mm x 8 mm in size, and is dominated by a large (approximately 9 mm x 5 mm) silicate nodule, which runs diagonally through the section and takes up 65% of the area (Figure 1). This nodule has a barred olivine texture, with olivine laths (Fo_{99}) typically 5 μm in width. The remainder of the section consists of chondrules (24 vol%), metal (10 vol%), and sulfide (1 vol%). Matrix metal grains typically range in size from 50 to 500 μm. Chondrule metal is smaller, limiting the possibility of LA-ICP-MS analysis, and only matrix metal was analyzed for trace elements. Sulfides, up to ~200 μm in size, are usually associated with metal. Smaller sulfide inclusions are frequently found within metal grains (Figure 2). Barred olivine, cryptocrystalline, and porphyritic chondrules are present in roughly equal proportions. Glass is present in many chondrules.

Analyses of matrix metal in GRO 95551 by LA-ICP-MS are listed in Table 1. The compositions of the matrix metal grains fell into two distinct groups. One, the "high-Ni" group, has about 7.2 ± 0.4 wt% Ni and 0.32 ± 0.02 wt% Co; metal in the other, "low-Ni" group has about 3.7 ± 0.1 wt% Ni and 0.45 ± 0.02 wt% Co (errors are 1 standard deviation). The high-Ni:low-Ni volume ratio of metal grains, based on point counting and EDX analyses of 46 grains in the section, is approximately 75:25. The number ratio of high-Ni:low-Ni grains is approximately 69:31, implying that the high-Ni metal grains may be larger on average than the low-Ni grains by ~35%, but this difference is within statistical error.

SEM analyses of the chondrule metal revealed a range of compositions, typically around 5-6 wt% Ni. Chikami and Miyamoto (1999) observed a negative correlation between Co and Ni in metal in GRO 95551, but they did not report the clustering into two metal compositions that is documented here. This suggests that Chikami and Miyamoto (1999) did not discriminate between the matrix metal and the chondrule metal, which does not fall into the same compositional clusters.

The low-Ni matrix metal grains have ~20 μm rims that are enriched in Ni relative to the interiors of the grains, reaching maximum Ni compositions of ~4.4 wt%. With the exception of these rims, the metal in each matrix metal grain appears to be homogeneous in Ni. To check for homogeneity of trace elements within the matrix metal grains in GRO 95551, two profiles of platinum group element (PGE) concentrations were obtained using LA-ICP-MS analyses with a 25 μm spot size. Ten and 14 measurements were made across a low-Ni grain and a high-Ni grain, respectively. No systematic variation of PGE contents with location within the grains was observed, and all of the measurements fell within 2σ error from the mean for each grain; therefore no heterogeneity of the PGEs was detected in these grains.

In Figure 3 the siderophile element compositions of the individual matrix metal grains in GRO 95551 are plotted against Ni. The high-Ni metal contains low P, Co, Ge

and As, and high Cu, Pd and Au relative to the low-Ni metal; the other siderophiles are less clearly fractionated between the two metal groups. The chromium content of the metal is strongly correlated with the sulfur content (Figure 4), and probably reflects the extent to which small sulfide inclusions were present in the ablated area of each grain (Figure 2). No other siderophile elements are correlated with S so strongly, indicating that only the Cr distribution is controlled primarily by the presence of sulfides.

The average GRO 95551 matrix metal composition (Table 1) was calculated from the observed modality of high-Ni and low-Ni metal and the average composition for each group; this result is normalized to Ni and CI chondrites in Figure 5. Normalized in this way, it is seen that in GRO 95551 metal the refractory siderophiles, with the exception of W and Re, are nearly unfractionated from one another and are depleted relative to Ni by 35-45%. The volatile elements As, Cu, Ga, Sb, Ge, and Sn are also depleted, roughly according to their volatility. The weighted Co/Ni ratio is about 22% higher than chondritic.

In Figure 3 the variability in refractory siderophile element (Mo, Ru, W, Re, Os, Ir, Pt) concentrations is very large among the grains, but the mean refractory contents are very similar between the high-Ni and low-Ni groups. Siderophile element compositions of individual grains are plotted against Ir in Figure 6. The refractory siderophiles Ru, Re, Os, and Pt are strongly correlated with Ir, but other siderophiles are not. Although Ir was used as an example in Figure 6, all of these elements correlate with one another, and similar figures could be produced with any of these refractory siderophiles as the abscissa.

Results for the ordinary chondrites, including 24 grains in Allegan, 5 in Soko-Banja, and 10 in Tieschitz, are given in Table 2, and plotted against Ni in Figure 7 and against Ir in Figure 8. Most analyses can be identified as either kamacite, with ~6 wt% Ni, or taenite, with >20 wt% Ni, but a few have intermediate Ni contents and can be inferred to have been mixtures of kamacite and taenite that were both overlapped by the laser ablation crater. Many of the siderophile-Ni relationships are similar to the data from GRO 95551 metal in that there is a large spread in the trace element concentration within each phase.

Strong correlations with Ni are observed for Pd and Au in all three meteorites (Figure 7). Figure 8 shows that the refractory siderophile elements Ru, Re, Os, Ir, and Pt are also strongly correlated with one another. Furthermore, these elements span a wide concentration range in the unequilibrated chondrites Tieschitz and Soko-Banja, but are more uniformly distributed among metal grains in the equilibrated chondrite Allegan, where much of the variation in refractory siderophiles corresponds to Ni content and appears to be related to kamacite/taenite partitioning (Figure 7).

4. DISCUSSION

4.1 History of Metal in GRO 95551

The relative abundances of minor and trace elements between the high-Ni and low-Ni metal groups in GRO 95551 (Figure 3) suggest that these two metal compositions were established by kamacite/taenite partitioning at high temperatures. Although most taenite in meteoritic metal contains high Ni contents (>20 wt%) due to continued equilibration during cooling, it can be seen from the Fe-Ni phase diagram (Chuang et al., 1986) that at higher temperatures, coexisting kamacite and taenite both have lower Ni contents than at low temperatures. The Ni contents of the two metal groups in GRO 95551 suggest equilibrium between the two phases at ~1020 K (Chuang et al., 1986); in contrast, iron meteorites display continued equilibration to <800 K (Narayan and Goldstein, 1985).

The high-Ni metal also contains low Co, As and P, and high Cu, Pd and Au relative to the low-Ni metal, and the refractory PGEs are nearly unfractionated between the two metal groups. This pattern is the same as one observes in kamacite/taenite partitioning in ordinary chondrites and iron meteorites (Rambaldi, 1976; Narayan and Goldstein, 1985; Campbell and Humayun, 1999b), although the degree of partitioning is lesser in GRO

95551, as one may expect if the metal phases equilibrated at higher temperature than is inferred from most meteoritic metal. At first glance Ge partitions contrary to expectation; it has been shown that at low temperatures in the Fe-Ni system Ge, like Ni, is enriched in taenite (fcc alloy) relative to kamacite (bcc alloy) (Goldstein, 1967), but in GRO 95551 Ge partitions into the low-Ni phase instead (Figure 3). This may result from differences in temperature and taenite composition; in the pure Fe-Ge system Ge partitions into the bcc phase, not the fcc phase, where the two coexist between 1185 and 1667 K (Kato and Nunoue, 1990). On the basis of both the Ni contents and the trace element abundances of the low-Ni and high-Ni metal phases in GRO 95551, we interpret these phases as the products of kamacite/taenite equilibration at ~1020 K, with rapid cooling from that temperature to prevent subsequent re-equilibration of the metal.

If the composition of the two metal groups reflects equilibrium at ~1020 K, then it should be expected that the silicate portion of GRO 95551 would exhibit equilibration at similar temperatures if the two components had cooled together in their present association. It is evident, however, that the chondrules in GRO 95551 have not equilibrated; many of them contain glass, indicating rapid quenching from high temperatures (e.g., ~1800 to 2100 K). Furthermore, the wide range of textures (barred olivine, cryptocrystalline, and porphyritic) and pyroxene compositions in the chondrules indicate that quenching occurred from a range of temperatures. It is conceivable that the observed excess W relative to the highly siderophile elements in GRO 95551 metal (Figure 5) could have been produced by reduction of silicates. The correlation between W and Mo (Figure 9) suggests that redox processes played a central role in establishing W and Mo contents in the metal, but this metal-silicate equilibrium could only have occurred in an early stage, before establishment of kamacite/taenite partitioning, because late stage equilibration of W and Mo between metal and silicates would also have permitted equilibration of W and Mo between the two metal phases, which is not observed.

Important constraints on the history of the components of GRO 95551 are placed by the observations that the matrix metal cooled quickly from ~1020 K, and the matrix metal and chondrules did not equilibrate at that temperature. Rapid cooling of the metal from ~1020 K follows from the fact that continued slow cooling would allow the kamacite and taenite to further equilibrate, and the Ni contents of both phases would have increased. A small amount of this continued re-equilibration to lower T may be seen in the rims of the low-Ni metal, in which the Ni content increases slightly over the outer 10-20 μm. It is also possible that these rims formed by a small degree of later oxidation. In either case, the lack of equivalent rims surrounding the high-Ni metal may simply be a consequence of slower diffusion in taenite than in kamacite (e.g., this difference in diffusion rates is responsible for the M-shaped profiles across taenite plates in octahedrite iron meteorites). The chondrules must have been mixed with the matrix metal after the kamacite/taenite partitioning was established in Ni and other elements; otherwise the silicates would show a greater degree of equilibration than is observed, and the chondrule metal would have equilibrated with the matrix metal.

One possible scenario is that the metal in GRO 95551 had been cooling slowly below the surface of a parent body, and was suddenly exposed when the temperature reached approximately 1020 K, perhaps as the result of impact-induced excavation of the overlying material. The chondrules could have been mixed with the metal at this time, and the mixture, which was then at or near the parent body surface, would have cooled too rapidly for continued re-equilibration of the metal and silicate phases. The metal in the chondrules would therefore have experienced a different thermal and chemical history than the matrix metal, as indicated by the observation that chondrule metal has a different distribution of Ni contents than matrix metal in GRO 95551. This scenario offers a natural way for other components, such as the dark inclusions (Weisberg et al., 2001), to have been added to the meteorite during regolith brecciation.

The wide range of refractory siderophile elements that is observed in both the high-Ni and low-Ni metal groups in GRO 95551 (Figure 3) is not consistent with complete equilibration between kamacite and taenite at ~1020 K or any other temperature. This variability in Ru, Re, Os, Ir, and Pt indicates that these elements were not efficiently transported between the two metal phases when Ni and other elements (e.g., Fe, Co, Cu, As, Pd, Au) were reaching kamacite/taenite equilibrium. One possible explanation is that the refractory PGEs did not diffuse through the metal rapidly enough to have attained their equilibrium concentrations in the metal phases. However, no diffusion-like profiles have been detected in refractory PGEs in these grains. Furthermore, differences in diffusion coefficients, such as those observed between Ru and Ir (Righter et al., 2002), would be expected to cause systematic deviations from chondritic relative abundances among the metal grains, in contrast with the observed correlations (Figure 6). An alternative interpretation of the lack of kamacite/taenite partitioning observed in Ru, Re, Os, Ir, and Pt (Figure 3) is that these elements were prevented from equilibrating between metal grains by an intervening phase such as sulfide, in which these elements are poorly soluble. For example, the metal grains may have been largely separated by a sulfide phase at high temperature, and this prevented transport of the most siderophile elements while allowing those elements that are more chalcophile (e.g., Fe, Co, Cu, As, Pd, Au) to attain equilibrium partitioning between the two metal phases. An obvious weakness of this model is that the current sulfide/metal ratio in the meteorite is too low for the sulfide to have reasonably surrounded most of the metal grains; the subsequent removal of a significant fraction of the sulfide is required for this model to work. Although the mechanism by which the refractory PGEs were prevented from equilibrating when other siderophiles were partitioning between kamacite and taenite remains uncertain, the existence of large, correlated variations in Ru, Re, Os, Ir, and Pt requires significant heterogeneity in the refractory siderophile content of the precursor metal to GRO 95551.

4.2 Comparison of GRO 95551 to Other Meteorite Groups

Weisberg et al. (2001) described the petrography of GRO 95551 as very similar to that of Bencubbin and Weatherford, with ~60% metal, large (cm-sized) metal and silicate clasts, and impact-produced melt areas between the metal and silicate. This is consistent with our observations of GRO 95551, although the section studied here was dominated by a single chondrule and was therefore probably not representative of the meteorite as a whole.

It was also shown by Weisberg et al. (2001) that GRO 95551 differs from Bencubbin in several important ways, including oxygen and nitrogen isotope compositions, presence of interstitial sulfides, and olivine compositions. To these differences we can add the siderophile element compositions of the metal (Figure 5). Bencubbin metal, taken as the average of analyses from Campbell et al. (2002), is enriched in refractory siderophiles (e.g., Ir) and strongly depleted in most volatile siderophiles (e.g., Ge), a chemical signature very different from that of GRO 95551. In particular, the relative lack of volatile siderophile depletions in GRO 95551 (Figure 5) is a feature that cannot be produced by subsolidus re-equilibration, and requires an origin distinct from that of metal in Bencubbin or related metal-rich meteorites, such as QUE 94411. Kallemeyn (2000) also concluded from preliminary INAA data for lithophile and volatile siderophile elements that GRO 95551 was compositionally distinct from the CB, CH, and CR meteorite groups, but the analytical results have not been published.

The average metal composition of GRO 95551 bears many similarities to that of equilibrated H chondrite metal, as shown in Figure 5. The Kong and Ebihara (1997) INAA data from metal separates was used in this figure instead of our new results on ordinary chondrite metal, because the wide variations in siderophile contents between grains (Figures 7 and 8) subjected the mean values of our limited number of analyses to sampling errors. The Ni-normalized refractory siderophile compositions in GRO 95551 are very

close to those of H metal, including the W and Re enrichments relative to other refractory siderophile elements. Both GRO 95551 metal and equilibrated H metal have volatile element concentrations that decrease with increasing volatility, although the volatile depletion is slightly greater in GRO 95551 metal. Some moderately siderophile elements, including Fe and Ga, are higher in GRO 95551 metal than in H metal, reflecting the higher degree of oxidation in H chondrites. (Bulk metals in L and LL chondrites have similar trends to the H metal, but with progressively greater depletions in oxidizable elements such as W, Mo, and Fe.) Apart from these explainable differences, the metal in GRO 95551 is more comparable to that of ordinary chondrites than to any other meteorite group. This, in addition to the similarity in their oxygen isotope compositions (Weisberg et al., 2001), suggests a possible genetic link between GRO 95551 and ordinary chondrites. Since oxygen isotopes reflect the provenance of the silicate fraction, the present study of the metal composition indicates that metal and silicate may be from related reservoirs, and that unlike mesosiderites (for example) these do not require an extraneous metal source.

To further illustrate the compositional differences involving the relative contributions of refractory and volatile siderophile elements, the chondrite-normalized Au/Ir ratio is plotted against the Ni content of metal from various chondrite types in Figure 10. The carbonaceous chondrite metal from CRs (Kong et al., 1999) and CBs (Campbell et al., 2002) exhibits low $(Au/Ir)_N$ since volatile Au is generally depleted, and refractory Ir is either at or above chondritic abundances. Enstatite chondrite metal (Kong et al., 1997) reflects the general depletion of refractory siderophiles relative to Ni evident in enstatite chondrite bulk compositions (Hertogen et al., 1983; Horan et al., 2002) and the enhancement of the Au/Ni ratio that is uniquely characteristic of E chondrites (Hertogen et al., 1983). Enstatite chondrite metal, CB and CR metal, and GRO 95551 metal all share similarly low Ni contents, which reflects the fact that all chondrite types share the same bulk Fe/Ni ratio (Wasson and Kallemeyn, 1988), and that under reducing conditions most of the Fe is sequestered in Fe-Ni alloy. This property distinguishes metal in GRO 95551

from that in H, L and LL chondrites, which exhibit progressive oxidation with the highest Ni contents in LL chondrite metal. Thus, while GRO 95551 metal evidently shares the genetic cosmochemical features of H, L and LL metal represented by the $(Au/Ir)_N$ ratio, it represents a new chondrite type with affinity to the ordinary chondrites, but more reduced than H chondrites.

The observed reduced state of GRO 95551 metal, and the high metal/silicate ratio, is particularly interesting given the high W/Ir and Re/Ir ratios, similar to that of H6 metal (Figure 5). This feature requires that the W was introduced to the metal by reduction of an initially oxidized precursor (W in silicate), and further, that the metal/silicate ratio was similar to that of H chondrites at the time of this reduction, as indicated by the magnitude of the W anomaly in Figure 5. A similar sequence is imagined for Re, but with less Re in the oxidized precursor, producing a smaller Re anomaly (Figure 5). The ratio $(W/Fe)_N = 1.22$ is nearly chondritic, and the bulk W abundance of the metal is 0.55 ppm (Table 1), which is about half that observed in H chondrite metal (Humayun and Campbell, 2002) and consistent with the difference in Fe/Ni ratios.

In addition to the high Fe/Ni ratio and reduced silicate composition (Fa ~ 1.3 mol%; Weisberg et al., 2001), important differences between GRO 95551 and the ordinary chondrites include an enhanced metal/silicate ratio, a greater proportion of barred olivine and cryptocrystalline chondrules, and lack of a fine-grained matrix. These latter textural characteristics are reminiscent of Bencubbin-like meteorites, which are known to be chondritic breccias. The constraints on GRO 95551 evolution include that the matrix metal and chondrules do not appear to have equilibrated, which taken together with the presence of dark inclusions of distinct oxygen isotopic composition (Weisberg et al., 2001), implies that GRO 95551, like Bencubbin, is also a breccia. It is possible that impact sorting during brecciation produced the high metal/silicate ratio.

4.3. Platinum Group Element Variations Among Individual Metal Grains in Ordinary Chondrites and GRO 95551

In Allegan (H5) the Ni compositions of the metal represent kamacite (Ni-poor) and taenite (Ni-rich), and the range of Ni compositions observed in these two phases is limited (Table 2; Figure 7). Tieschitz (H3.6) and Soko-Banja (LL4) display a wider range of compositions within the kamacite or taenite groupings, and this is consistent with the interpretation of these meteorites as being less equilibrated than Allegan. Furthermore, the mean kamacite composition is higher, and the mean taenite compositions lower, in Allegan than in Tieschitz, also indicating that the metal in Allegan has equilibrated at higher temperature than in Tieschitz.

The elements Pd and Au are like Ni in that they are nonrefractory, highly siderophile, and partition into taenite, and they are distributed in all ordinary chondrite metal in the same way as Ni (Figure 7). Likewise, in Allegan, an equilibrated chondrite, the refractory siderophiles Mo, Ru, W, Re, Os, Ir, and Pt have partitioned between kamacite and taenite in a manner consistent with that observed in octahedrite iron meteorites (Campbell and Humayun, 1999b). In contrast, the distributions of refractory siderophiles in the unequilibrated meteorites Tieschitz and Soko-Banja appear to be unrelated to kamacite/taenite partitioning (Figure 7), and therefore these elements may hold clues to the pre-equilibration history of the ordinary chondrites.

Earlier work (Hsu et al., 1998; Humayun and Campbell, 2000; 2002) also showed that refractory siderophile element compositions vary greatly between individual metal grains in unequilibrated ordinary chondrites. Humayun and Campbell (2002) focussed in particular on the large variations in the W/Ir ratio in unequilibrated chondrites, and concluded that this variability disappeared via reduction of W during initial metamorphism of the parent bodies. Similar results for W can be seen in Figures 7 and 8; in Tieschitz and Soko-Banja metal W is highly variable, but in the equilibrated chondrite Allegan W

concentrations are more restricted, with a small degree of preferential partitioning of W into the kamacite phase. Molybdenum behaves in a similar fashion to W in ordinary chondrite metal, although the spread in the Allegan Mo data may be larger than that of the W data (Figures 7 and 11). There is one Mo measurement in Allegan that is exceptionally high, and it is possible that the data were affected by small inclusions of an unidentified Mo-rich phase within the metal. Unlike the GRO 95551 metal (Figure 9), ordinary chondrite metal does not exhibit a strong correlation between Mo and W concentrations (Figure 11).

In Figure 8 it is demonstrated that the variations in the refractory, highly siderophile elements Ru, Re, Os, Ir, and Pt are not independent of one another but are instead correlated over ~3 orders of magnitude variation in Ir. In OC metal the Os/Ir ratio is tightly constrained regardless of the Ni content or degree of equilibration, whereas there are small but significant variations in the Re/Ir and Pt/Ir ratios, and at low Ir contents (<1 ppm) the Ru/Ir ratio deviates greatly from that at higher Ir contents (Figure 8). These observations are reminiscent of similar correlations found over a more limited compositional range in GRO 95551 metal (Figure 6).

The correlated variations of refractory metals among metal grains in unequilibrated ordinary chondrites and GRO 95551 suggest that a refractory component is heterogeneously distributed in these metal grains. A similar conclusion was reached by Grossman and Wasson (1985), who observed variable PGE/Ni ratios among chondrules from Semarkona (LL3.0). Grossman and Wasson (1985) attributed this to refractory condensate metal that was variably mixed with refractory-depleted metal in chondrule precursors. In one such model, a population of grains bearing highly variable refractory/volatile contents, due to different evaporation/condensation histories, may have aggregated in varying proportions to form a number of grain clusters, which were then melted in a chondrule-forming thermal event (perhaps a shock wave, for example (Desch and Connolly, 2002)). This interpretation is consistent with the present data set, which includes several highly siderophile, less refractory elements such as Pd and Au that do not

follow the pattern of distribution exhibited by the refractory siderophiles (Figure 8). The correlated Mo and W abundances in GRO 95551 metal (Figure 9) imply that the refractory component entering this metal may have been variably oxidized, which could explain the variation in the W-Ir and Mo-Ir plots (Figure 6). An analogous model for the formation of metal in refractory inclusions in CV chondrites was discussed by Campbell et al. (2003) on the basis of trace siderophile element distributions in the refractory metal.

Another class of models calls for the formation of metal primarily by reduction of silicate during chondrule melting (Zanda et al., 1994; Connolly et al., 1994, 2001; Lauretta et al., 2001). The establishment of refractory element correlations in these models is more complicated in light of the present data because nonrefractory siderophiles such as Pd and Au would be expected to correlate with the refractory PGEs, but they do not (Figure 8). Microanalysis of metal in Renazzo chondrules (Connolly et al., 2001; Humayun et al., 2002; Zanda et al., 2002) has established the importance of recondensation of metal that had volatilized from chondrules, which combined with metal formed by chondrule reduction may produce the observed siderophile distributions in ordinary chondrite matrix metal. (The redox conditions of CR metal formation, and that of OC metal formation are different, however, as noted in the discussion of Figure 10.) A possible scenario is that Pd and Au may have volatilized with Fe and Ni during chondrule melting and evaporation, and then recondensed at approximately uniform concentration levels on metal grains that were variably enriched in the refractory PGEs because of varying degrees of volatilization. Verification of this model should include careful study of the HSE distribution in highly unequilibrated chondrites.

5. CONCLUSIONS

The two distinct compositional groups of matrix metal in GRO 95551 reflect kamacite/taenite partitioning at relatively high temperatures, ~1020 K, as indicated by the abundances of Ni and other nonrefractory siderophile elements in the metal. This metal was subsequently cooled at a rate rapid enough to prevent significant re-equilibration of the metal. The refractory siderophile elements do not display kamacite/taenite partitioning, but instead show correlated intergrain variations in GRO 95551 metal, indicating variations in refractory metal content that were not erased during equilibration at ~1020 K.

The bulk composition of GRO 95551 metal is significantly more refractory depleted, and less volatile depleted, than other metal-rich chondrites such as those of the CB and CH groups to which it has been previously compared. Bulk GRO 95551 metal does, however, have strong compositional similarities to that of H chondrites, which further strengthens the association implied by the oxygen isotope data (Weisberg et al., 2001). Despite the chemical similarities between H chondrite metal and that of GRO 95551, this meteorite is not simply a misclassified ordinary chondrite, but instead represents a new chondrite type with affinity to the ordinary chondrites.

Unequilibrated ordinary chondrite metal shows correlated intergrain variations in the refractory siderophile elements Ru, Re, Os, Ir, and Pt that are even larger than those observed in GRO 95551, but these correlations are not observed in the nonrefractory siderophile elements Pd and Au, and this has important genetic implications. Metal formation strictly by reduction and removal from chondrules can be eliminated by these results, but to resolve between origins involving heterogeneous chondrule precursors or reduction, melting, and evaporation/recondensation of chondrules, future work should focus on the measurement of siderophile element abundances in relation to the position of the metal grains within or around unmetamorphosed chondrules.

Acknowledgments–We are grateful to the Meteorite Working Group for providing the section of GRO 95551, to M. Wadhwa at the Field Museum of Natural History for providing specimens of Allegan and Soko-Banja, and to G. Kurat at the Naturhistorisches Museum Wien for the section of Tieschitz. The manuscript benefitted from reviews by H. C. Connolly, Jr., T. Schönbeck, an anonymous reviewer, and the associate editor, H. Palme. This work was supported by NASA through grant NAG 5-9800 to M. H.

REFERENCES

Anders E. and Grevesse N. (1989) Abundances of the elements: Meteoritic and solar. *Geochim. Cosmochim. Acta* **53**, 197-214.

Campbell A. J. and Humayun M. (1999a) Trace element microanalysis in iron meteorites by laser ablation ICPMS. *Anal. Chem.* **71**, 939-946.

Campbell A. J. and Humayun M. (1999b) Microanalysis of platinum group elements in iron meteorites using laser ablation ICP-MS. In *Lunar and Planetary Science XXX*, Abstract #1974, Lunar and Planetary Institute, Houston (CD-ROM).

Campbell A. J., Humayun M. and Weisberg M. K. (2000) Siderophile element distributions in zoned metal grains in Hammadah al Hamra 237. *Meteorit. Planet. Sci.* **35**, A38-A39.

Campbell A. J., Humayun M., Meibom A., Krot A. N. and Keil K. (2001) Origin of zoned metal grains in the QUE94411 chondrite. *Geochim. Cosmochim. Acta* **65**, 163-180.

Campbell A. J. and Humayun M. (2002a) Condensation of metal in a CH chondrite. *Meteorit. Planet. Sci.* **37**, A29 (abstr.).

Campbell A. J. and Humayun M. (2002b) Siderophile element distributions in the metal-rich chondrite GRO 95551. In *Lunar and Planetary Science XXXIII*, Abstract #1842, Lunar and Planetary Institute, Houston (CD-ROM).

Campbell A. J., Humayun M. and Weisberg M. K. (2002) Siderophile element constraints on the formation of metal in the metal-rich chondrites Bencubbin, Weatherford, and Gujba. *Geochim. Cosmochim. Acta* **66**, 647-660.

Campbell A. J., Simon S. B., Humayun M. and Grossman L. (2003) Chemical evolution of metal in refractory inclusions in CV3 chondrites. *Geochim. Cosmochim. Acta* **67**, in press.

Chikami J. amd Miyamoto M. (1999) Mineralogical study of Grosvenor Mountains 95551 chondrite in comparison with the CR-clan chondrites. *Meteorit. Planet. Sci.* **34**, A24-25 (abstr.).

Chuang Y.-Y., Chang Y. A., Schmid R. and Lin J.-C. (1986) Magnetic contributions to the thermodynamic functions of alloys and the phase equilibria of Fe-Ni system below 1200 K. *Metall. Trans. A, 17A,* 1361-1372.

Connolly H. C., Jr., Hewins R. H., Ash R. D., Zanda B., Lofgren G. E. and Bourot-Denise M. (1994) Carbon and the formation of reduced chondrules. *Science* **371**, 136-139.

Connolly H. C., Jr., Huss G. R. and Wasserburg G. J. (2001) On the formation of Fe-Ni metal in Renazzo-like carbonaceous chondrites. *Geochim. Cosmochim. Acta* **65**, 4567-4588.

Desch S. J. and Connolly H. C., Jr. (2002) A model of the thermal processing of particles in solar nebula shocks: Application to the cooling rates of chondrules. *Meteorit. Planet. Sci.* **37**, 183-207.

Goldstein J. T. (1967) Distribution of germanium in the metallic phases of some iron meteorites. *J. Geophys. Res.* **72**, 4689-4696.

Grossman L. and Olsen E. (1974) Origin of the high-temperature fraction of C2 chondrites. *Geochim. Cosmochim. Acta* **38**, 173-187.

Grossman J. N. and Wasson J. T. (1983) Refractory precursor components of Semarkona chondrules and the fractionation of refractory elements among chondrites. *Geochim. Cosmochim. Acta* **47**, 759-771.

Grossman J. N. and Wasson J. T. (1985) The origin and history of the metal and sulfide components of chondrules. *Geochim. Cosmochim. Acta* **49**, 925-939.

Hertogen J., Janssens M.-J., Takahashi H., Morgan J. W. and Anders E. (1983) Enstatite chondrites: Trace element clues to their origin. *Geochim. Cosmochim. Acta* **47**, 2241-2255.

Horan M. F., Walker R. J., Morgan J. W., Grossman J. N. and Rubin A. E. (2002) Highly siderophile elements in chondrites. *Chem. Geol*. (submitted).

Hsu W., Huss G. R. and Wasserburg G. J. (1998) Ion probe analyses of PGEs in metallic phases of chondrites: Implications for the origin of chondritic metals. In *Lunar and Planetary Science XXIX*, Abstract #1939, Lunar and Planetary Institute, Houston (CD-ROM).

Humayun M. and Campbell A. J. (2000) Re, Os, and Ir fractionation in ordinary chondrite metal. In *Lunar and Planetary Science XXXI*, Abstract #2032, Lunar and Planetary Institute, Houston (CD-ROM).

Humayun M. and Campbell A. J. (2002) The duration of ordinary chondrite metamorphism inferred from tungsten microdistribution in metal. *Earth Planet. Sci. Lett*. **198**, 225-243.

Humayun M., Campbell A. J., Zanda B., and Bourot-Denise M. (2002) Formation of Renazzo chondrule metal inferred from siderophile elements. In *Lunar and Planetary Science XXXIII*, Abstract #1965, Lunar and Planetary Institute, Houston (CD-ROM).

Jones R. H. (1994) Petrology of FeO-poor, porphyritic pyroxene chondrules in the Semarkona chondrite. *Geochim. Cosmochim. Acta* **58**, 5325-5340.

Kallemeyn G. W. (2000) The composition of the Grosvenor Mountains 95551 anomalous chondrite and its relationship to other reduced chondrites. *Meteorit. Planet. Sci.* **35**, A85 (abstr.).

Kato E. and Nunoue S. (1990) Fe-Ge (iron-germanium). In *Binary Alloy Phase Diagrams*, ed. Massalski T. B. et al., ASM International.

Kong P. and Ebihara M. (1997) The origin and nebular history of the metal phase of ordinary chondrites. *Geochim. Cosmochim. Acta* **61**, 2317-2329.

Kong P., Mori T. and Ebihara M. (1997) Compositional continuity of enstatite chondrites and implications for heterogeneous accretion of the enstatite chondrite parent body. *Geochim. Cosmochim. Acta* **61**, 4895-4914.

Kong P., Ebihara M. and Palme H. (1999) Distribution of siderophile elements in CR chondrites: Evidence for evaporation and recondensation during chondrule formation. *Geochim. Cosmochim. Acta* **63**, 2637-2652.

Lauretta D. S., Buseck P. R. and Zega T. J. (2001) Opaque minerals in the matrix of Bishunpur (LL3.1) chondrite: Constraints on the chondrule formation environment. *Geochim. Cosmochim. Acta* **65**, 1337-1353.

Mason B. (1997) Petrographic description of GRO 95551. *Ant. Meteorit. Newslet.* **20**, 11.

Meibom A., Petaev M. I., Krot A. N., Wood J. A. and Keil K. (1999) Primitive FeNi metal grains in CH carbonaceous chondrites formed by condensation from a gas of solar composition. *J. Geophys. Res.* **104**, 22053-22059.

Meibom A., Desch S. J., Krot A. N., Cuzzi J. N., Petaev M. I., Wilson L. and Keil K. (2000) Large scale thermal events in the solar nebula recorded in Fe, Ni metal condensates in primitive meteorites. *Science* **288**, 839-841.

Narayan C. and Goldstein J. I. (1985) A major revision of the iron meteorite cooling rates - An experimental study of the growth of the Widmanstätten pattern. *Geochim. Cosmochim. Acta* **49**, 397-410.

Newsom H. E. and Drake M. J. (1979) The origin of metal clasts in the Bencubbin meteorite breccia. *Geochim. Cosmochim. Acta* **43**, 689-707.

Petaev M. I., Meibom A., Krot A. N., Wood J. A. and Keil K. (2001) The condensation origin of zoned metal grains in Queen Alexandra Range 94411: Implications for the formation of the Bencubbin-like chondrites. *Meteorit. Planet. Sci.* **36**, 93-106.

Rambaldi E. (1976) Trace element content of metals from L-group chondrites. *Earth Planet. Sci. Lett.* **31**, 224-238.

Righter K., Campbell A. J. and Humayun M. (2002) Diffusion in metal: Application to zoned metal grains in chondrites. *Geochim. Cosmochim. Acta* **66**, A639 (abstr.).

Wasson J. T. and Kallemeyn G. W. (1988) Compositions of chondrites. *Phil. Trans. R. Soc. London A* **325**, 535-544.

Weisberg M. K., Prinz M., Clayton R. N. and Mayeda T. K. (1993) The CR (Renazzo-type) carbonaceous chondrite group and its implications. *Geochim. Cosmochim. Acta* **57**, 1567-1586.

Weisberg M. K., Prinz M., Clayton R. N., Mayeda T. K., Sugiura N., Zashu S. and Ebihara M. (1999) QUE94411 and the origin of bencubbinites. In *Lunar and Planetary Science XXX*, Abstract #1416, Lunar and Planetary Institute, Houston (CD-ROM).

Weisberg M. K., Prinz M., Clayton R. N., Mayeda T. K., Sugiura N., Zashu S. and Ebihara M. (2001) A new metal-rich chondrite group. *Meteorit. Planet. Sci*. **36**, 401-418.

Zanda B., Bourot-Denise M., Perron C. and Hewins R. H. (1994) Origin and metamorphic redistribution of silicon, chromium, and phosphorus in the metal of chondrites. *Science* **265**, 1846-1849.

Zanda B., Bourot-Denise M., Hewins R. H., Cohen B. A., Delaney J. S., Humayun M. and Campbell A. J. (2002) Accretion textures, iron evaporation and re-condensation in Renazzo chondrules. In *Lunar and Planetary Science XXXIII*, Abstract #1852, Lunar and Planetary Institute, Houston (CD-ROM).

Table 1. LA-ICP-MS analyses of individual matrix metal grains in GRO 95551. Italics denote detection limits. Data in ppm unless otherwise noted.

grain#	P, wt%	S	V	Cr	Fe, wt%	Co, wt%	Ni, wt%	Cu	Ga	Ge	As
high-Ni											
5	0.186 ± 0.006	673 ± 22	*1.0*	410 ± 13	92 ± 3	0.327 ± 0.010	7.68 ± 0.23	180 ± 5	18.8 ± 0.6	29.8 ± 0.9	5.3 ± 0.3
6	0.338 ± 0.010	323 ± 12	*2.5*	82 ± 3	92 ± 3	0.329 ± 0.010	7.78 ± 0.23	153 ± 5	16.1 ± 0.5	33.8 ± 1.1	3.9 ± 0.4
8	0.153 ± 0.005	275 ± 9	*2.3*	180 ± 6	93 ± 3	0.302 ± 0.009	6.66 ± 0.20	163 ± 5	16.5 ± 0.5	31.7 ± 1.1	5.1 ± 0.4
9	0.128 ± 0.004	1321 ± 40	2.20 ± 0.09	1607 ± 49	93 ± 3	0.303 ± 0.009	6.98 ± 0.21	186 ± 6	19.3 ± 0.6	29.7 ± 0.9	5.2 ± 0.2
11	0.145 ± 0.004	533 ± 18		452 ± 14	92 ± 3	0.316 ± 0.009	7.61 ± 0.23				
13	0.185 ± 0.006	369 ± 16	*2.8*	377 ± 12	93 ± 3	0.282 ± 0.008	6.63 ± 0.20	140 ± 4	14.5 ± 0.5	35.0 ± 1.2	4.9 ± 0.5
14	0.251 ± 0.008	239 ± 15	*2.8*	76 ± 5	93 ± 3	0.329 ± 0.010	6.91 ± 0.21	156 ± 5	16.4 ± 0.6	29.6 ± 1.0	4.5 ± 0.5
16	0.214 ± 0.006	193 ± 8	*2.2*	51 ± 2	92 ± 3	0.322 ± 0.010	7.26 ± 0.22	150 ± 5	14.7 ± 0.5	35.4 ± 1.2	5.1 ± 0.4
19	0.175 ± 0.005	168 ± 7	2.50 ± 0.09	46 ± 2	93 ± 3	0.327 ± 0.010	7.05 ± 0.21	174 ± 5	18.9 ± 0.6	31.8 ± 1.0	5.7 ± 0.2
24	0.243 ± 0.007	*115*	*2.4*	41 ± 4	92 ± 3	0.330 ± 0.010	7.26 ± 0.22	131 ± 4	15.3 ± 0.5	29.6 ± 1.0	5.5 ± 0.4
low-Ni											
1	0.368 ± 0.011	202 ± 11	4.25 ± 0.15	29 ± 3	96 ± 3	0.473 ± 0.014	3.76 ± 0.11	94 ± 3	18.7 ± 0.6	37.3 ± 1.2	8.6 ± 0.3
7	0.340 ± 0.010	288 ± 14	*2.3*	50 ± 4	96 ± 3	0.438 ± 0.013	3.65 ± 0.11	86 ± 3	15.3 ± 0.5	48.6 ± 1.6	7.7 ± 0.5
15	0.475 ± 0.014	128 ± 12	*2.2*	52 ± 4	96 ± 3	0.483 ± 0.015	3.53 ± 0.11	80 ± 3	15.5 ± 0.5	41.1 ± 1.3	7.9 ± 0.5
18	0.329 ± 0.010	171 ± 7	1.16 ± 0.06	54 ± 2	96 ± 3	0.437 ± 0.013	4.00 ± 0.12	93 ± 3	18.9 ± 0.6	37.9 ± 1.2	8.3 ± 0.3
21	0.393 ± 0.012	164 ± 7	3.86 ± 0.17	37 ± 2	96 ± 3	0.444 ± 0.013	3.72 ± 0.11	107 ± 3	15.5 ± 0.5	41.4 ± 1.3	7.0 ± 0.4
22	0.382 ± 0.011	340 ± 11	*2.0*	300 ± 9	96 ± 3	0.456 ± 0.014	3.76 ± 0.11	80 ± 3	14.9 ± 0.5	44.8 ± 1.4	7.6 ± 0.4
23	0.447 ± 0.013	*106*	*2.0*	38 ± 3	96 ± 3	0.442 ± 0.013	3.61 ± 0.11	84 ± 3	17.0 ± 0.6	48.6 ± 1.5	8.3 ± 0.4
bulk average											
	0.245	389	2.84	270	93	0.351	6.31	142	16.7	34.6	5.7

grain#	Mo	Ru	Pd	Sn	Sb	W	Re	Os	Ir	Pt	Au
high-Ni											
5	3.6 ± 0.3	3.3 ± 0.2	3.9 ± 0.2	0.84 ± 0.12	0.21 ± 0.02	0.51 ± 0.06	0.20 ± 0.04	2.06 ± 0.11	1.96 ± 0.09	3.55 ± 0.19	0.94 ± 0.06
6	4.0 ± 0.3	4.3 ± 0.2	3.9 ± 0.2	*1.1*	*0.1*	0.61 ± 0.06	0.43 ± 0.04	3.19 ± 0.14	2.38 ± 0.10	4.78 ± 0.22	0.79 ± 0.05
8	2.5 ± 0.1	2.0 ± 0.1	2.6 ± 0.1	*1.0*	0.19 ± 0.04	0.40 ± 0.04	0.10 ± 0.01	1.19 ± 0.06	0.99 ± 0.05	1.82 ± 0.09	0.78 ± 0.04
9	3.7 ± 0.2	3.3 ± 0.2	3.2 ± 0.2	0.73 ± 0.10	0.25 ± 0.02	0.51 ± 0.05	0.24 ± 0.03	2.56 ± 0.11	2.53 ± 0.10	4.31 ± 0.20	0.80 ± 0.05
11	4.4 ± 0.3	2.7 ± 0.2	3.9 ± 0.2			0.44 ± 0.05	0.13 ± 0.02	1.90 ± 0.10	1.51 ± 0.08	3.35 ± 0.18	0.83 ± 0.06
13	2.9 ± 0.3	1.6 ± 0.2	2.9 ± 0.3	*1.3*	0.21 ± 0.05	0.35 ± 0.06	*0.05*	1.25 ± 0.09	1.01 ± 0.07	1.60 ± 0.14	0.78 ± 0.07
14	2.4 ± 0.3	2.8 ± 0.3	2.9 ± 0.3	*1.2*	0.20 ± 0.05	0.40 ± 0.08	0.18 ± 0.04	1.64 ± 0.12	1.58 ± 0.10	3.75 ± 0.25	0.98 ± 0.09
16	3.6 ± 0.2	2.8 ± 0.2	3.2 ± 0.2	*1.0*	0.14 ± 0.04	0.74 ± 0.07	0.23 ± 0.03	2.18 ± 0.11	1.99 ± 0.09	3.72 ± 0.18	0.62 ± 0.05
19	3.4 ± 0.2	2.0 ± 0.1	3.5 ± 0.2	0.61 ± 0.09	0.27 ± 0.02	0.55 ± 0.05	0.10 ± 0.02	1.36 ± 0.07	1.21 ± 0.06	2.04 ± 0.12	0.74 ± 0.05
24	3.0 ± 0.3	2.5 ± 0.3	3.0 ± 0.3	*1.1*	0.14 ± 0.04	0.34 ± 0.07	0.17 ± 0.04	1.84 ± 0.12	1.56 ± 0.10	3.25 ± 0.22	0.78 ± 0.07
low-Ni											
1	4.7 ± 0.3	2.2 ± 0.2	1.9 ± 0.2	1.47 ± 0.13	0.26 ± 0.03	0.86 ± 0.08	0.11 ± 0.03	0.68 ± 0.06	0.84 ± 0.05	2.75 ± 0.16	0.62 ± 0.05
7	3.1 ± 0.3	2.7 ± 0.2	1.8 ± 0.2	*1.0*	0.19 ± 0.04	0.50 ± 0.07	0.15 ± 0.03	1.76 ± 0.12	1.66 ± 0.10	2.75 ± 0.19	0.74 ± 0.07
15	2.9 ± 0.3	2.4 ± 0.2	1.2 ± 0.2	*1.0*	0.20 ± 0.04	0.34 ± 0.07	0.19 ± 0.04	2.08 ± 0.13	1.86 ± 0.11	3.80 ± 0.25	0.56 ± 0.06
18	4.1 ± 0.2	2.5 ± 0.2	2.0 ± 0.1	0.84 ± 0.10	0.29 ± 0.02	0.74 ± 0.06	0.22 ± 0.03	1.82 ± 0.09	1.79 ± 0.08	3.17 ± 0.15	0.51 ± 0.04
21	4.1 ± 0.2	2.8 ± 0.2	2.0 ± 0.1	*1.0*	0.14 ± 0.04	0.66 ± 0.06	0.18 ± 0.02	1.92 ± 0.09	1.83 ± 0.08	3.41 ± 0.16	0.57 ± 0.04
22	3.9 ± 0.2	2.8 ± 0.2	1.7 ± 0.1	*0.9*	0.18 ± 0.04	0.77 ± 0.06	0.16 ± 0.02	2.08 ± 0.09	1.96 ± 0.08	3.37 ± 0.16	0.46 ± 0.03
23	4.0 ± 0.3	2.9 ± 0.3	1.2 ± 0.2	*0.9*	0.21 ± 0.04	0.47 ± 0.07	0.26 ± 0.04	2.31 ± 0.14	2.21 ± 0.12	4.31 ± 0.26	0.52 ± 0.06
bulk average											
	3.5	2.6	2.8	0.83	0.20	0.555	0.17	1.85	1.64	3.15	0.75

Table 2. LA-ICP-MS analyses of individual matrix metal grains in ordinary chondrites. Data in ppm unless otherwise noted.

	V	Cr	Fe (wt%)	Co (wt%)	Ni (wt%)	Ge	Mo	Ru	Pd	W	Re	Os	Ir	Pt	Au
Allegan															
#4			76 ± 2	0.173 ± 0.005	24.0 ± 0.7		5.2 ± 0.4	9.0 ± 0.6	12.3 ± 0.7	0.40 ± 0.10	0.65 ± 0.07	2.87 ± 0.19	2.82 ± 0.17	11.6 ± 0.6	1.54 ± 0.12
#5		38 ± 4	93 ± 3	0.482 ± 0.014	6.2 ± 0.2		4.0 ± 0.4	5.9 ± 0.5	3.2 ± 0.3	0.53 ± 0.12	0.26 ± 0.04	6.23 ± 0.40	4.34 ± 0.26	8.2 ± 0.4	0.78 ± 0.07
#6	21.8 ± 1.4	1249 ± 45	70 ± 2	0.145 ± 0.004	29.5 ± 0.9		4.5 ± 0.4	9.0 ± 0.6	20.0 ± 1.1	0.33 ± 0.09	0.77 ± 0.08	3.58 ± 0.23	2.97 ± 0.18	11.6 ± 0.6	2.30 ± 0.18
#8		44 ± 3	91 ± 3	0.429 ± 0.013	5.6 ± 0.2		6.5 ± 0.5	2.0 ± 0.2	2.3 ± 0.2	0.60 ± 0.12	0.09 ± 0.01	1.25 ± 0.09	1.27 ± 0.08	9.8 ± 0.5	0.78 ± 0.06
#14	1.2 ± 0.3	25 ± 4	93 ± 3	0.539 ± 0.016	6.0 ± 0.2		58.1 ± 2.1	6.1 ± 0.6	2.4 ± 0.3	0.75 ± 0.12	0.36 ± 0.06	5.97 ± 0.31	5.54 ± 0.27	7.7 ± 0.5	0.52 ± 0.08
#16		353 ± 14	93 ± 3	0.457 ± 0.014	6.2 ± 0.2		4.1 ± 0.2	2.4 ± 0.3	2.1 ± 0.3	0.77 ± 0.12	0.22 ± 0.03	1.27 ± 0.07	1.23 ± 0.06	8.1 ± 0.5	0.58 ± 0.08
#17		59 ± 5	92 ± 3	0.509 ± 0.015	6.7 ± 0.2		5.7 ± 0.3	2.7 ± 0.3	2.4 ± 0.3	0.61 ± 0.10	0.21 ± 0.03	2.00 ± 0.11	1.09 ± 0.05	6.0 ± 0.4	0.80 ± 0.11
#18	1.8 ± 0.3	31 ± 4	93 ± 3	0.473 ± 0.014	6.9 ± 0.2		4.3 ± 0.2	2.4 ± 0.3	3.0 ± 0.4	0.66 ± 0.10	0.29 ± 0.04	1.80 ± 0.10	1.37 ± 0.07	4.6 ± 0.3	0.80 ± 0.11
#22	79.9 ± 4.7	4415 ± 155	71 ± 2	0.164 ± 0.005	28.7 ± 0.9		7.1 ± 0.3	9.5 ± 0.8	16.6 ± 1.9	0.69 ± 0.11	0.52 ± 0.07	3.34 ± 0.18	3.41 ± 0.17	15.3 ± 0.9	2.46 ± 0.30
#23	1.1 ± 0.3	145 ± 7	92 ± 3	0.488 ± 0.015	7.6 ± 0.2		4.6 ± 0.2	3.2 ± 0.3	3.3 ± 0.4	0.64 ± 0.10	0.14 ± 0.02	1.08 ± 0.06	0.93 ± 0.05	7.4 ± 0.4	0.53 ± 0.08
#24	1.8 ± 0.3	311 ± 12	92 ± 3	0.538 ± 0.016	6.9 ± 0.2		6.0 ± 0.3	3.0 ± 0.3	2.5 ± 0.3	0.73 ± 0.11	0.16 ± 0.02	1.26 ± 0.07	1.22 ± 0.06	9.0 ± 0.5	1.18 ± 0.15
#25	1.7 ± 0.3	191 ± 9	75 ± 2	0.178 ± 0.005	24.6 ± 0.7		7.5 ± 0.3	6.8 ± 0.6	14.9 ± 1.7	0.41 ± 0.07	0.51 ± 0.07	2.46 ± 0.13	2.22 ± 0.11	10.3 ± 0.6	1.71 ± 0.21
#26	27.5 ± 1.8	2673 ± 95	85 ± 3	0.502 ± 0.015	13.5 ± 0.4		3.0 ± 0.3	2.4 ± 0.3	4.1 ± 0.5	0.68 ± 0.12	0.30 ± 0.04	2.49 ± 0.13	2.30 ± 0.11	8.2 ± 0.5	0.88 ± 0.12
#27	42.4 ± 2.7	334 ± 15	85 ± 3	0.541 ± 0.016	14.6 ± 0.4		1.8 ± 0.3	3.4 ± 0.4	5.7 ± 0.7	0.70 ± 0.13	0.35 ± 0.05	1.92 ± 0.10	2.04 ± 0.10	5.5 ± 0.3	1.39 ± 0.19
#28	49.8 ± 3.2	324 ± 15	91 ± 3	0.610 ± 0.018	8.0 ± 0.2			3.2 ± 0.5	2.6 ± 0.4	0.58 ± 0.12	0.33 ± 0.05	2.43 ± 0.13	2.48 ± 0.12	4.7 ± 0.3	0.83 ± 0.13
#29	15 ± 13	688 ± 627	93 ± 3	0.464 ± 0.019	6.2 ± 0.3		4.1 ± 0.2	3.3 ± 0.2	2.4 ± 0.1	0.68 ± 0.05	0.17 ± 0.01	1.66 ± 0.07	1.38 ± 0.09	4.0 ± 0.3	0.67 ± 0.04
#30	12.9 ± 0.5	482 ± 15	94 ± 3	0.467 ± 0.014	5.8 ± 0.2		4.0 ± 0.3	3.6 ± 0.3	2.8 ± 0.2	0.78 ± 0.09	0.25 ± 0.04	1.62 ± 0.10	1.47 ± 0.09	5.4 ± 0.3	0.75 ± 0.06
#31	12.4 ± 0.5	251 ± 8	93 ± 3	0.478 ± 0.014	6.4 ± 0.2		2.8 ± 0.2	3.4 ± 0.3	2.5 ± 0.2	0.63 ± 0.08	0.13 ± 0.03	1.00 ± 0.08	0.83 ± 0.06	6.3 ± 0.3	0.50 ± 0.05
#32	16.3 ± 0.6	935 ± 28	93 ± 3	0.473 ± 0.014	6.2 ± 0.2		3.6 ± 0.2	3.3 ± 0.3	2.7 ± 0.2	0.58 ± 0.07	0.28 ± 0.04	1.89 ± 0.11	1.83 ± 0.10	5.3 ± 0.3	0.64 ± 0.05
#33	3.4 ± 0.2	132 ± 5	94 ± 3	0.484 ± 0.015	5.9 ± 0.2		7.5 ± 0.4	2.6 ± 0.2	2.8 ± 0.2	0.71 ± 0.08	0.29 ± 0.04	0.86 ± 0.07	1.30 ± 0.08	3.0 ± 0.2	0.41 ± 0.04
#34	22.0 ± 0.7	869 ± 26	73 ± 2	0.142 ± 0.004	27.3 ± 0.8		8.8 ± 0.4	15.7 ± 0.7	12.9 ± 0.6	0.67 ± 0.07	0.61 ± 0.05	7.24 ± 0.28	7.78 ± 0.28	29.1 ± 1.0	1.83 ± 0.09
#35	1.16 ± 0.15	133 ± 5	69 ± 2	0.141 ± 0.004	31.3 ± 0.9		7.9 ± 0.4	12.1 ± 0.6	18.0 ± 0.7	1.79 ± 0.12	0.71 ± 0.06	8.06 ± 0.30	5.10 ± 0.20	24.0 ± 0.8	2.32 ± 0.11
#36	1.05 ± 0.13	27 ± 2	71 ± 2	0.130 ± 0.004	29.2 ± 0.9		4.6 ± 0.3	13.9 ± 0.6	12.0 ± 0.5	0.55 ± 0.06	0.64 ± 0.05	6.39 ± 0.25	6.34 ± 0.23	18.0 ± 0.6	1.94 ± 0.09
#37	0.60 ± 0.14	19 ± 2	76 ± 2	0.162 ± 0.005	23.8 ± 0.7		5.4 ± 0.3	13.1 ± 0.6	11.9 ± 0.5	0.60 ± 0.07	0.61 ± 0.06	4.42 ± 0.19	5.00 ± 0.20	16.9 ± 0.6	1.38 ± 0.08
Soko-Banja															
#1	102 ± 3	5440 ± 165	63 ± 2	0.359 ± 0.011	35.1 ± 1.1		6.4 ± 0.5	20.1 ± 1.1	18.3 ± 1.0	0.62 ± 0.14	1.07 ± 0.15	10.4 ± 0.5	8.31 ± 0.36	22.0 ± 1.0	3.20 ± 0.21
#2	74 ± 2	3242 ± 98	64 ± 2	0.445 ± 0.013	35.1 ± 1.1		4.4 ± 0.3	17.5 ± 0.8	14.5 ± 0.7	0.73 ± 0.09	1.09 ± 0.08	7.43 ± 0.32	6.99 ± 0.27	18.9 ± 0.7	2.42 ± 0.12
#3	1.9 ± 0.3	33 ± 4	73 ± 2	1.225 ± 0.037	26.0 ± 0.8		8.7 ± 0.6	7.2 ± 0.6	12.8 ± 0.7	1.58 ± 0.18	0.59 ± 0.08	5.44 ± 0.33	4.80 ± 0.26	11.4 ± 0.6	1.16 ± 0.09
#4	3.2 ± 0.3	110 ± 5	64 ± 2	0.562 ± 0.017	35.8 ± 1.1		5.2 ± 0.4	1.5 ± 0.3	17.7 ± 0.9	0.41 ± 0.10	0.05 ± 0.03	0.38 ± 0.10	0.25 ± 0.05	2.4 ± 0.3	1.98 ± 0.12
#5	22.2 ± 0.7	766 ± 23	88 ± 3	1.806 ± 0.054	10.6 ± 0.3		6.3 ± 0.3	14.8 ± 0.6	4.0 ± 0.2	0.18 ± 0.03	1.41 ± 0.08	16.4 ± 0.5	16.7 ± 0.5	28.2 ± 0.9	0.79 ± 0.05
Tieschitz															
#1		3119 ± 97	56 ± 2	0.203 ± 0.006	41.0 ± 1.2		9.9 ± 0.8	7.7 ± 0.8	26.4 ± 1.5	0.67 ± 0.12	0.39 ± 0.08	5.98 ± 0.34	4.49 ± 0.25	8.1 ± 0.5	
#2		601 ± 19	94 ± 3	0.563 ± 0.017	5.1 ± 0.2		1.5 ± 0.2	4.4 ± 0.4	1.6 ± 0.2	0.96 ± 0.08	0.32 ± 0.04	3.19 ± 0.16	3.21 ± 0.14	5.9 ± 0.3	
#3			93 ± 3	0.741 ± 0.022	5.4 ± 0.2	59 ± 3		1.7 ± 0.4	2.6 ± 0.4	0.08 ± 0.04		0.03 ± 0.02	0.03 ± 0.01	0.2 ± 0.1	
#4		1960 ± 66	94 ± 3	0.848 ± 0.026	5.2 ± 0.2	51 ± 4		4.3 ± 1.0	0.9 ± 0.5			1.65 ± 0.22	1.43 ± 0.17	4.1 ± 0.5	
#5		956 ± 32	92 ± 3	0.821 ± 0.025	7.1 ± 0.2	66 ± 3		6.6 ± 0.7	3.4 ± 0.5		0.77 ± 0.10	5.05 ± 0.29	4.43 ± 0.24	10.3 ± 0.6	
#6			93 ± 3	0.852 ± 0.026	5.4 ± 0.2	62 ± 3		2.1 ± 0.4	1.0 ± 0.2	0.86 ± 0.11	0.28 ± 0.05	1.69 ± 0.14	1.88 ± 0.13	3.5 ± 0.3	
#7		2954 ± 91	96 ± 3	0.789 ± 0.024	3.3 ± 0.1	46 ± 2	7.9 ± 0.6	6.4 ± 0.7	0.7 ± 0.2	0.22 ± 0.06	0.41 ± 0.07	4.57 ± 0.27	3.81 ± 0.21	9.4 ± 0.5	
#8			92 ± 3	0.618 ± 0.019	6.9 ± 0.2	43 ± 2		3.3 ± 0.5	2.0 ± 0.4			0.06 ± 0.03	0.16 ± 0.04	0.6 ± 0.1	
#9			50 ± 2	0.124 ± 0.004	50.7 ± 1.5	133 ± 5		1.7 ± 0.3	29.0 ± 1.5				0.02 ± 0.01	0.4 ± 0.1	
#10		391 ± 14	90 ± 3	0.718 ± 0.022	9.1 ± 0.3	67 ± 3	3.4 ± 0.4	2.7 ± 0.4	2.8 ± 0.4		0.38 ± 0.06	1.93 ± 0.15	2.29 ± 0.14	4.0 ± 0.3	

FIGURE CAPTIONS

Figure 1. Backscattered electron image of GRO 95551. The section is dominated by a large barred olivine chondrule; the rest of the section contains chondrules, Fe-Ni metal, and interstitial sulfides. Scale bar = 1 mm.

Figure 2. Backscattered electron image of GRO 95551. Sulfide inclusions are visible within some metal grains. Scale bar = 1 mm.

Figure 3. Siderophile element compositions in GRO 95551 metal plotted against Ni content. All abundances in ppm except Ni in wt%. The metal grains cluster into two groups having distinct Ni contents. Some elements partition between the two compositional groups, while others, particularly the refractory PGEs, show large variations and no correlation with Ni. The partitioning, when observed, is consistent with subsolidus partitioning between kamacite and taenite at ~1020 K. Dashed lines indicate CI ratios (Anders and Grevesse, 1989). Analytical errors (Table 1) are typically 5-10%.

Figure 4. Chromium and sulfur contents in GRO 95551 metal grains. The correlation between these two elements suggests that the Cr content is dominated by sulfide inclusions that are present in the grains. Analytical errors (Table 1) are smaller than the symbols.

Figure 5. Siderophile element abundance patterns of GRO 95551, H6 chondrite metal (Kong and Ebihara, 1997), and Bencubbin (Campbell et al., 2002), normalized to Ni and CI chondrites (Anders and Grevesse, 1989). The moderate depletions of both refractory and volatile siderophiles in GRO 95551 metal bear more resemblance to the metal in ordinary chondrites than to Bencubbin.

Figure 6. Siderophile element compositions in GRO 95551 metal plotted against Ir content. All abundances in ppm. The refractory siderophiles Ru, Re, Os, and Pt are strongly correlated with Ir, with nearly chondritic relative abundances of these elements in each grain. Dashed lines indicate CI ratios. Analytical errors (Table 1) are typically 5-10%.

Figure 7. Siderophile element compositions in ordinary chondrite metal plotted against Ni content. All abundances in ppm except Ni in wt%. In Allegan the siderophile elements correlate with Ni as a result of kamacite/taenite partitioning. In contrast, in the unequilibrated chondrites Soko-Banja and Tieschitz, the refractory siderophiles are poorly correlated with Ni, but Pd and Au are strongly correlated with Ni. Circles: Allegan H5; squares: Soko-Banja LL4; triangles: Tieschitz H3.6; dashed lines: CI ratios. Analytical errors (Table 1) are typically 5-10%.

Figure 8. Siderophile element compositions in ordinary chondrite metal plotted against Ir content. All abundances in ppm. Over variations in Ir of nearly three orders of magnitude, refractory siderophiles Ru, Re, Os, and Pt are correlated with Ir. Circles: Allegan H5; squares: Soko-Banja LL4; triangles: Tieschitz H3.6; dashed lines: CI ratios. Analytical errors (Table 1) are typically 5-10%.

Figure 9. Plot of W vs. Mo in GRO 95551 matrix metal grains. The correlation indicates that variations in redox conditions may have affected the refractory siderophile element distributions, causing the scatter in the Mo-Ir and W-Ir plots in Figure 8. Error bars are 1σ.

Figure 10. $(Au/Ir)_N$= chondrite normalized Au/Ir ratio vs. Ni content of bulk GRO 95551 metal (circle with cross) compared with LA-ICP-MS analyses of CB chondrite metal (filled diamonds) and bulk separated metals from the following chondrite types: H (open squares), L (open diamonds), LL (filled circles), EH (filled triangles), EL (open triangles),

CR (open circles). Data from Kong and Ebihara (1997), Kong et al. (1997), Kong et al. (1999) and Campbell et al. (2002). GRO 95551 metal shares the Au/Ir ratio of OC metal, but has Fe/Ni like CB, CR, EH and EL metal.

Figure 11. Plot of W vs. Mo in ordinary chondrite metal. Error bars are 1σ.

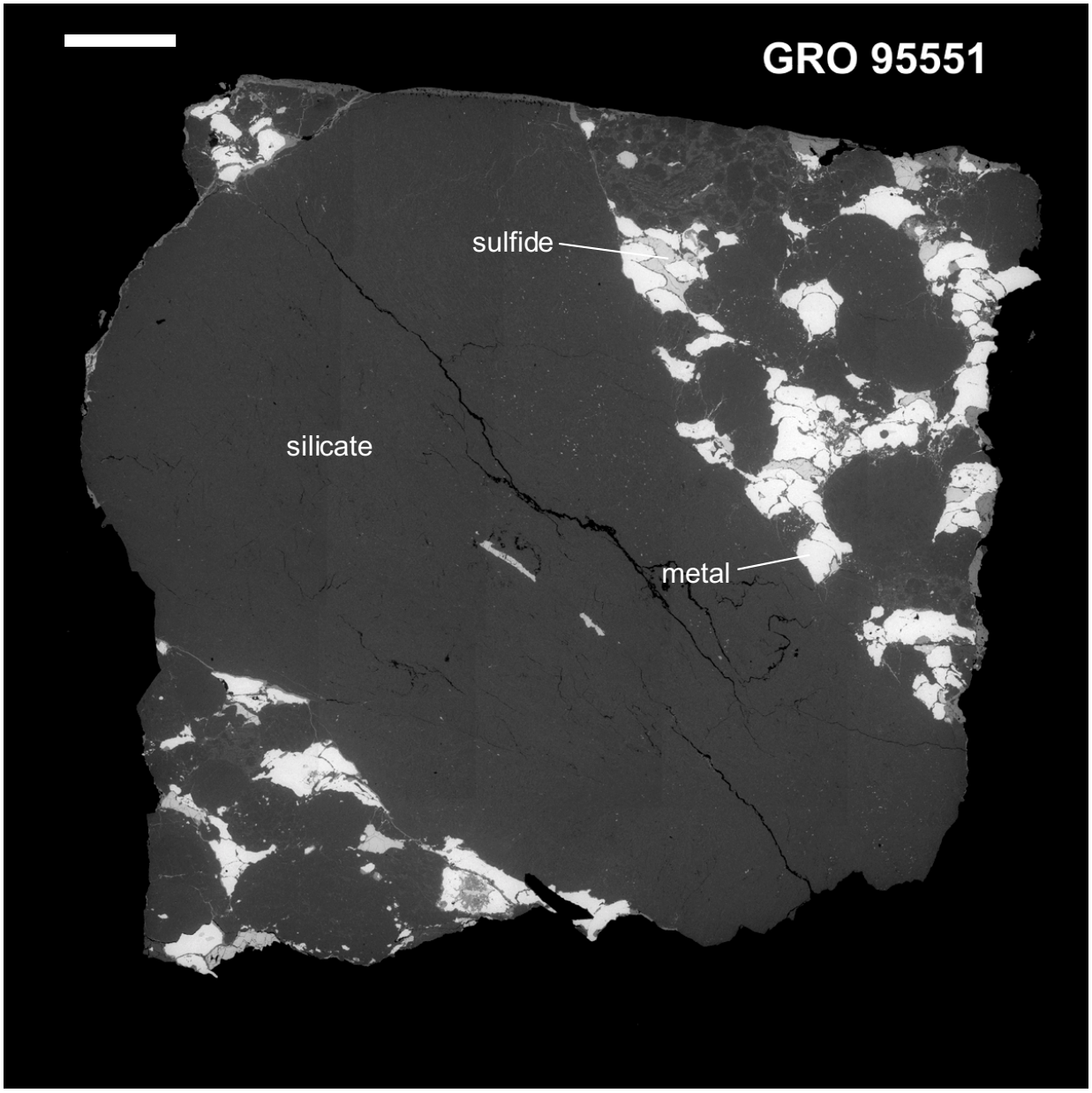

Figure 1

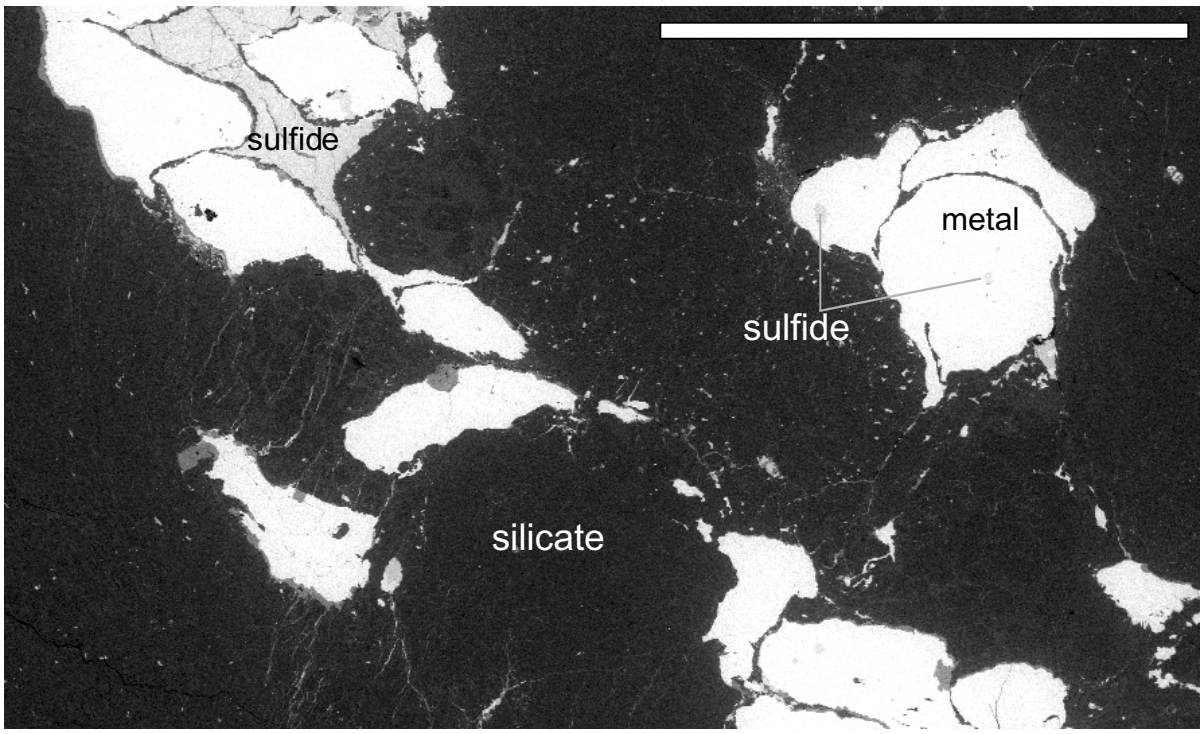

Figure 2

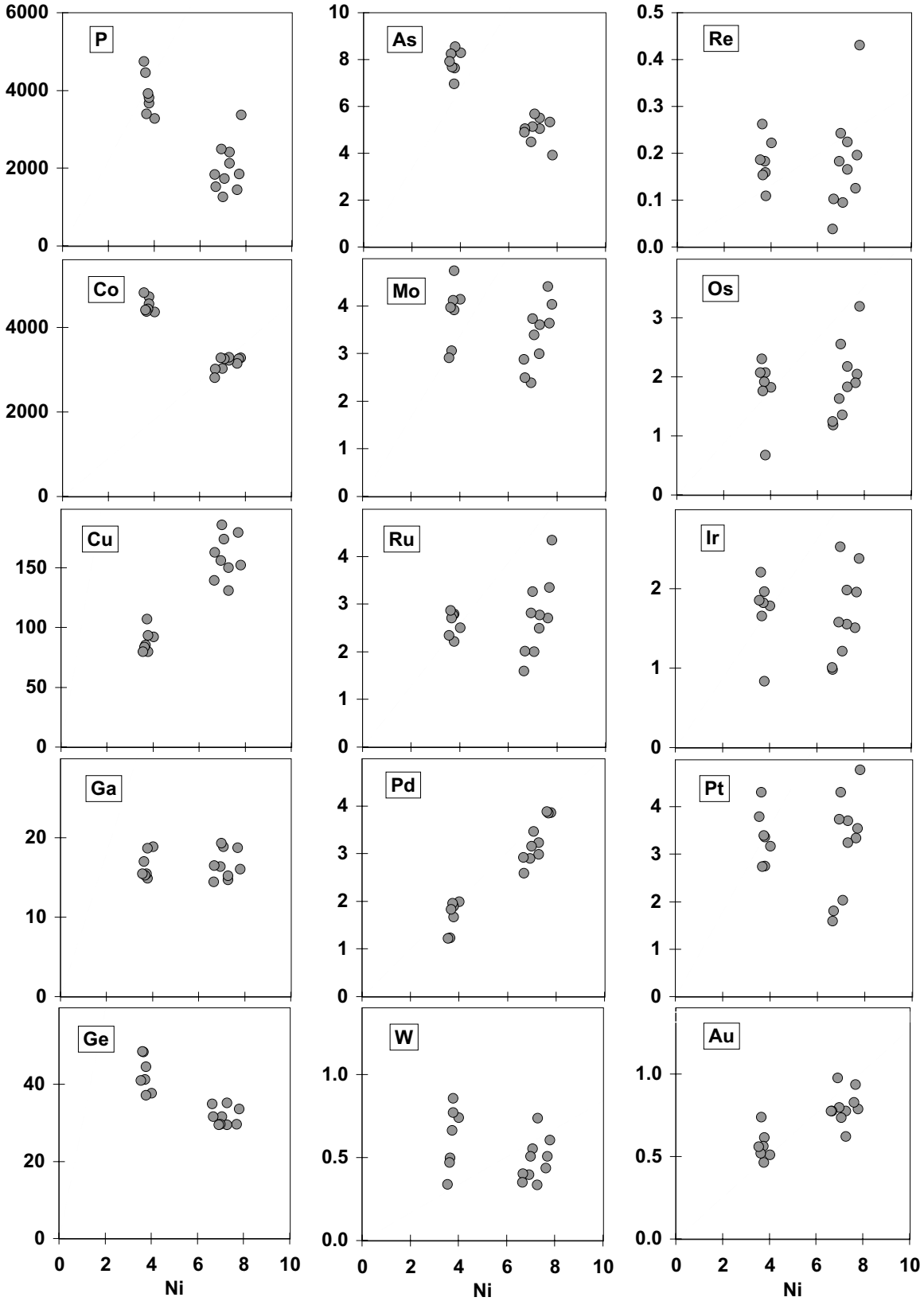

Figure 3

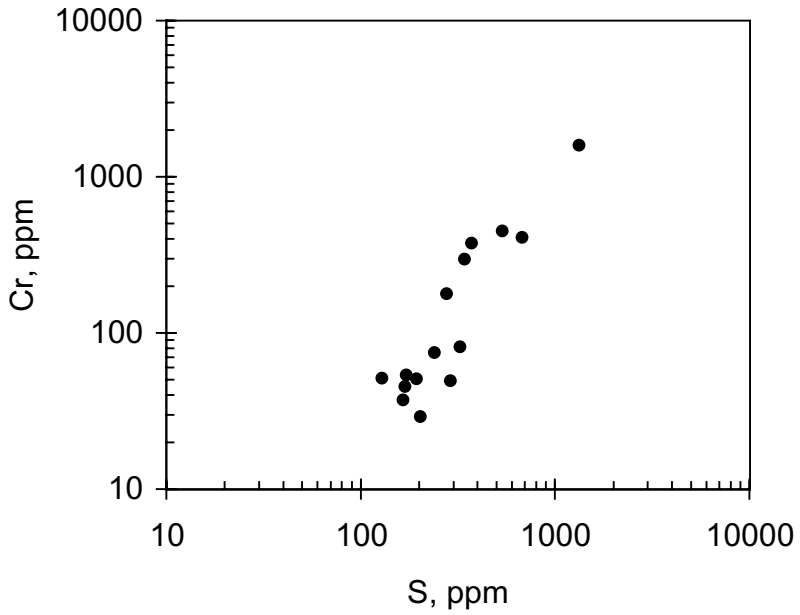

Figure 4

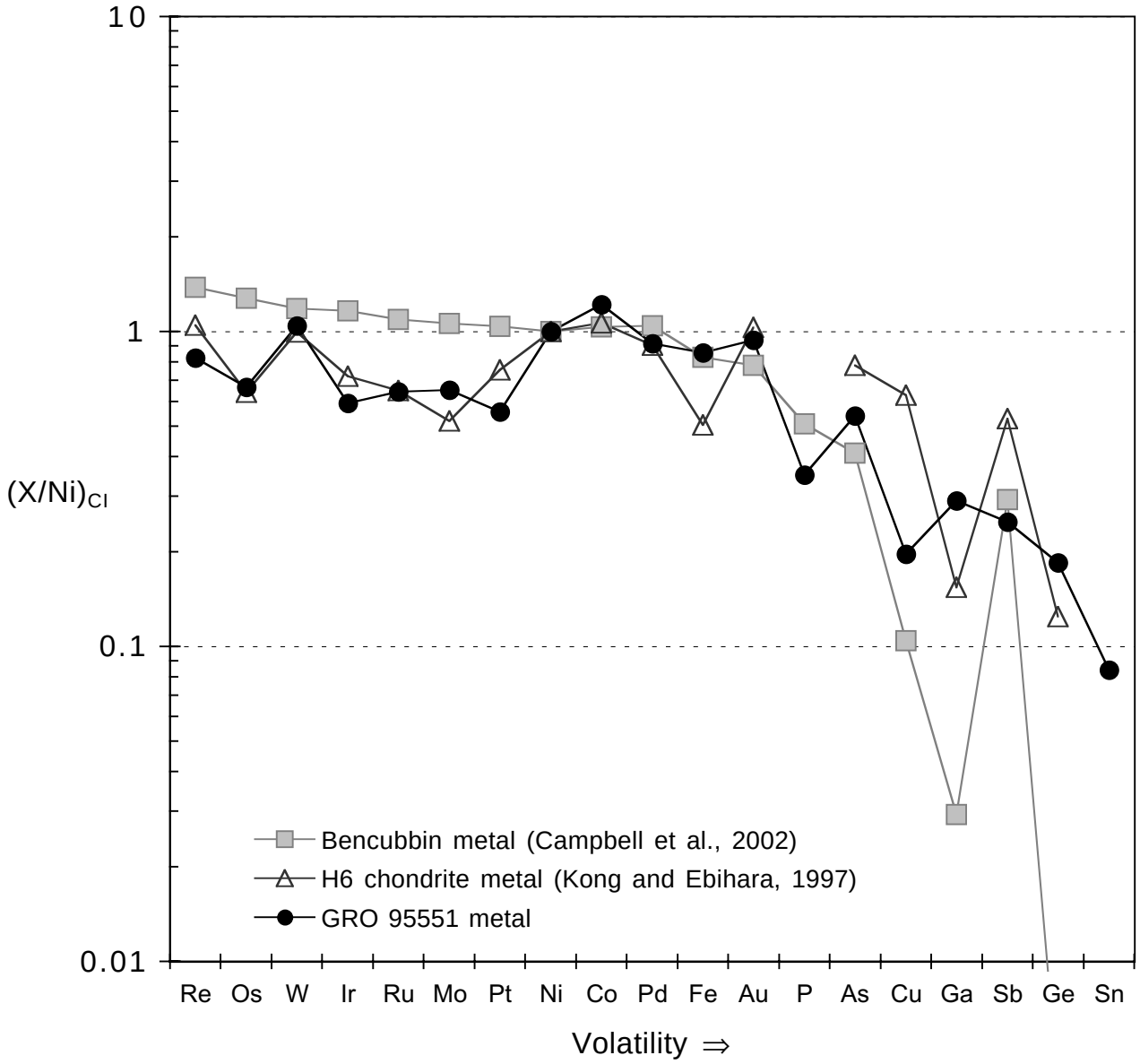
10
1
0.1
0.01
(X/Ni)CI
Bencubbin metal (Campbell et al., 2002)
H6 chondrite metal (Kong and Ebihara, 1997)
GRO 95551 metal
Re Os W Ir Ru Mo Pt Ni Co Pd Fe Au P As Cu Ga Sb Ge Sn
Volatility ⇒

Figure 5

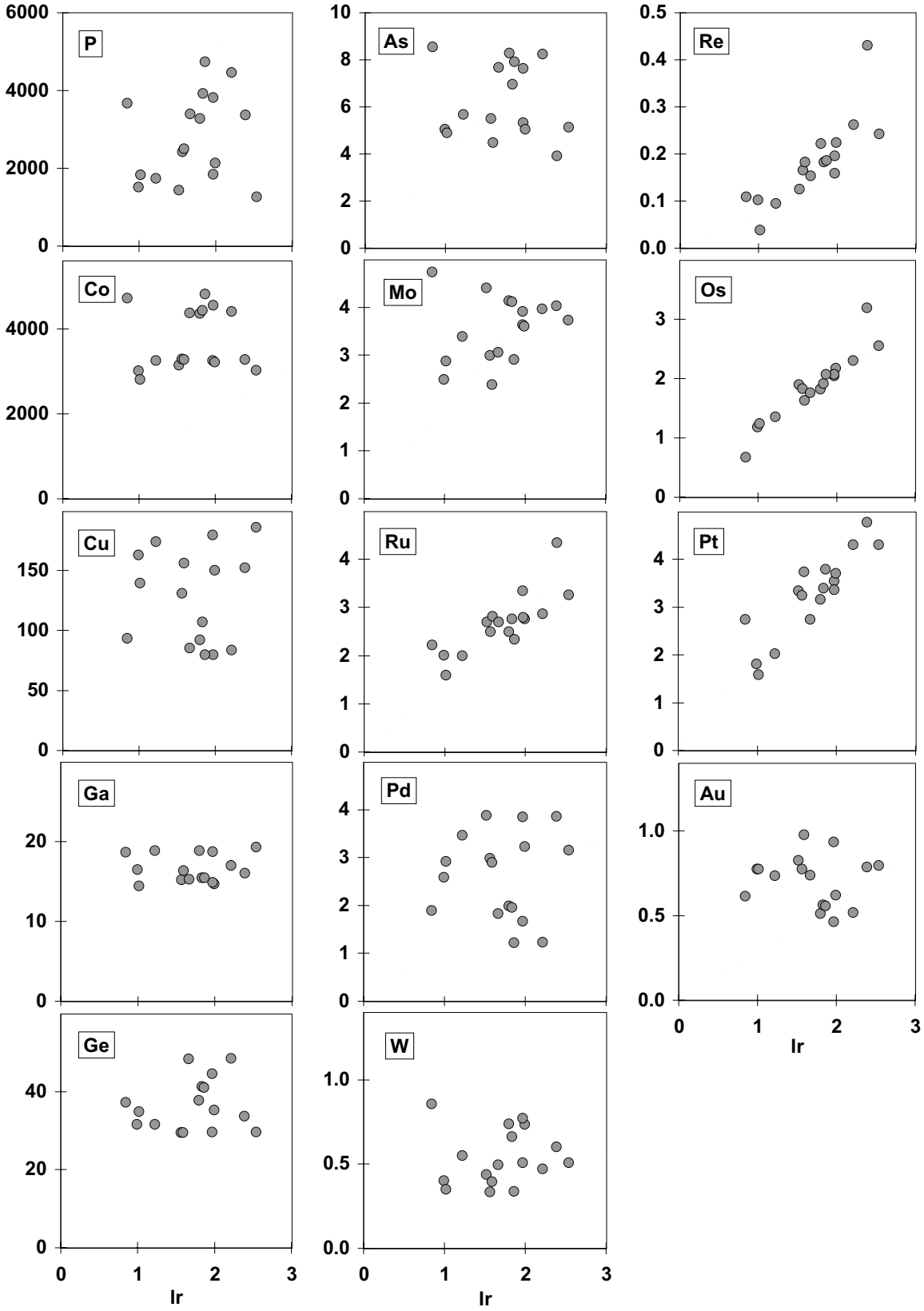

Figure 6

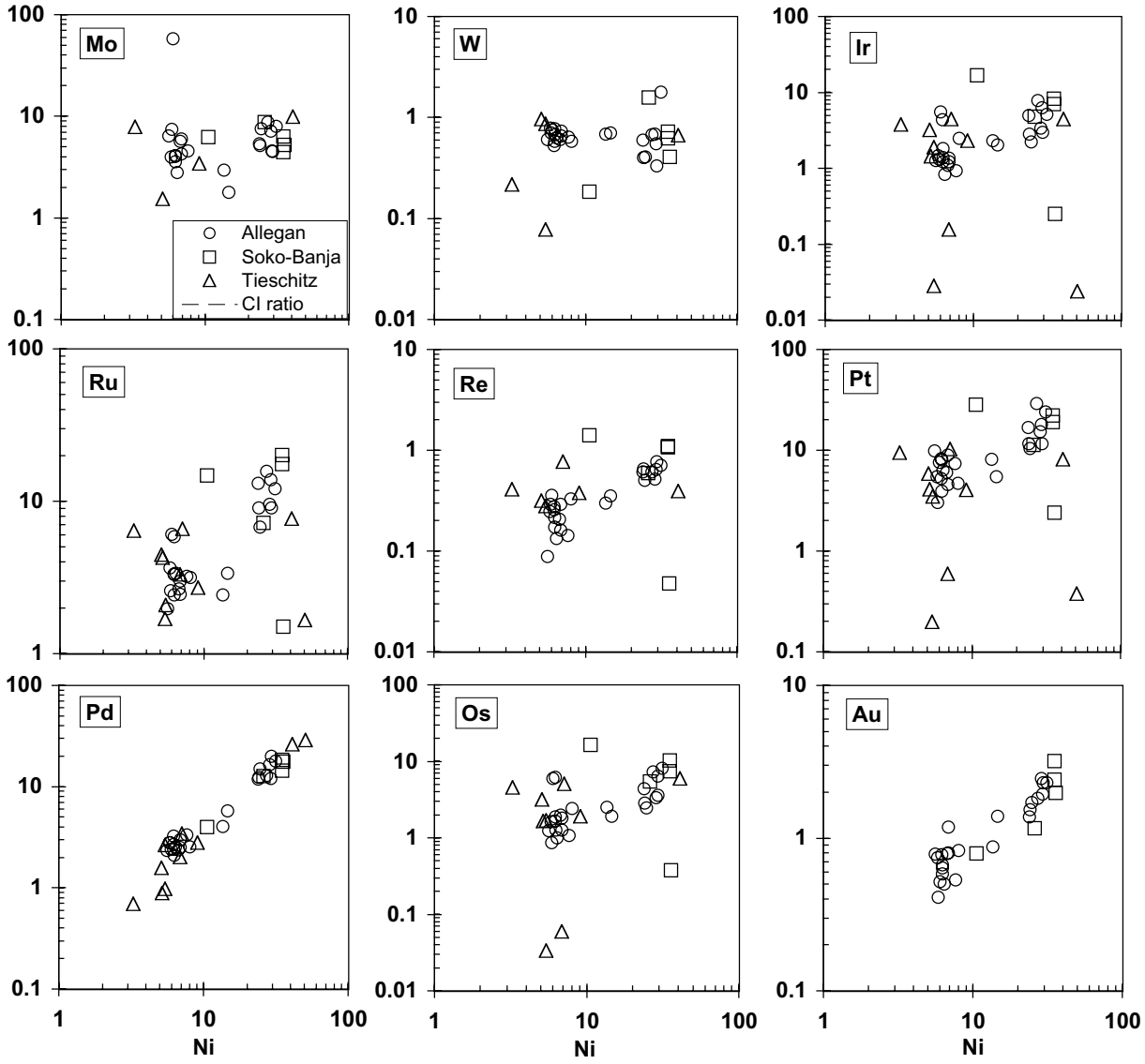
Mo
W
Ir
Ru
Re
Pt
Pd
Os
Au
Allegan
Soko-Banja
Tieschitz
CI ratio
Ni
Ni
Ni

Figure 7

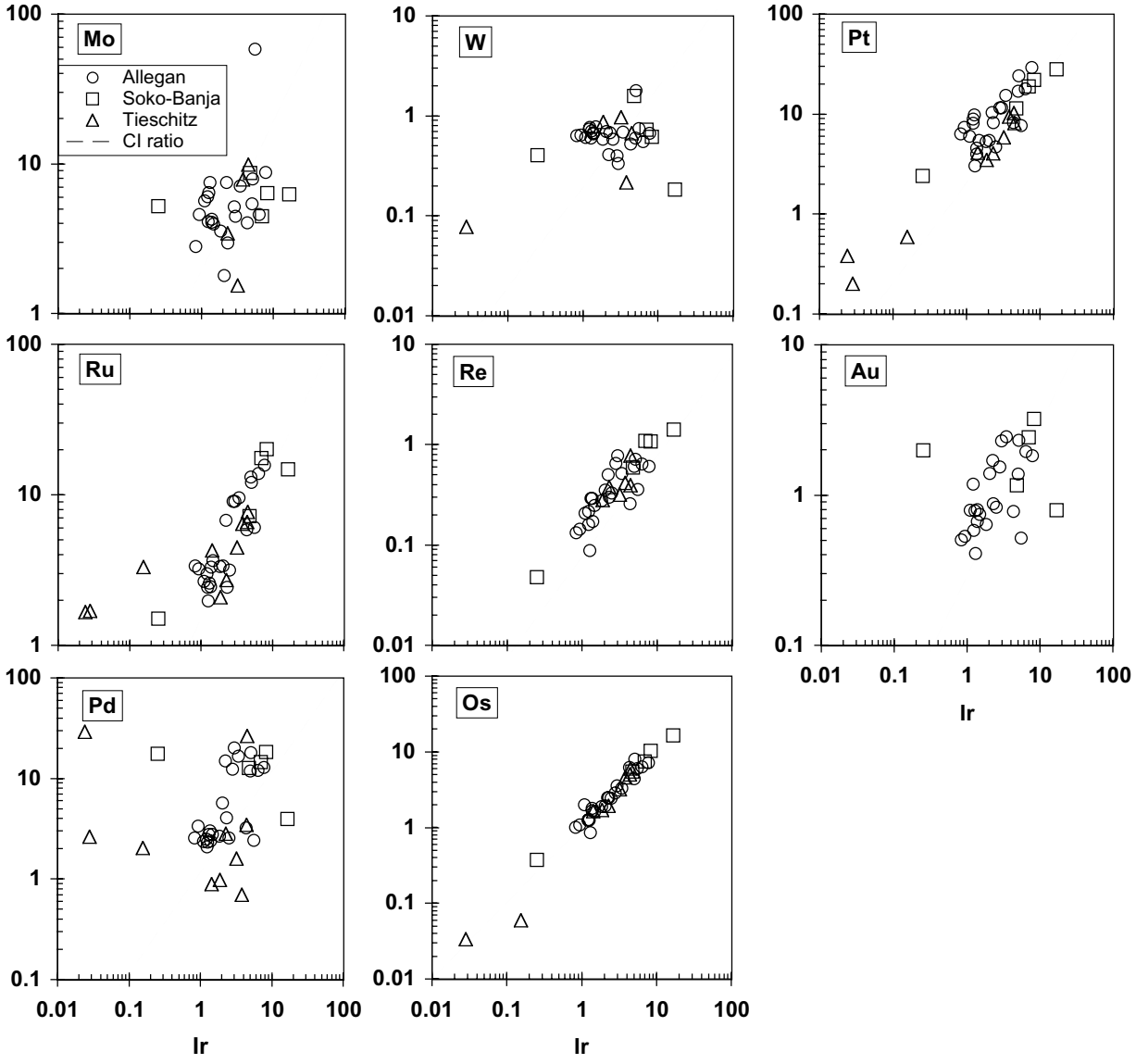
Mo
Allegan
Soko-Banja
Tieschitz
CI ratio
W
Pt
Ru
Re
Au
Pd
Os
Ir
Ir
100
10
1
0.1
0.01

Figure 8

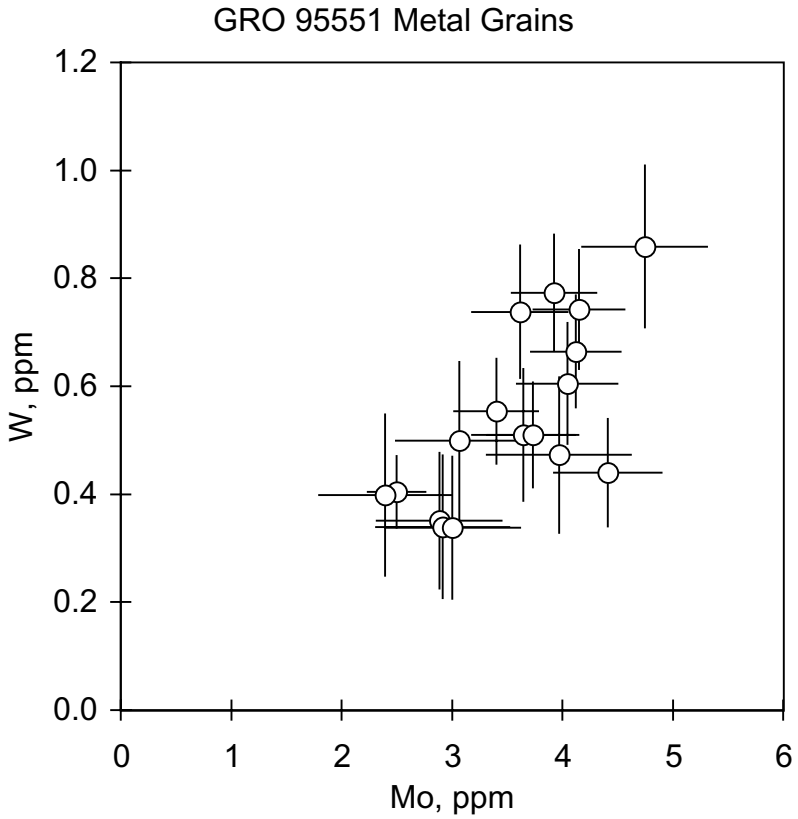

Figure 9

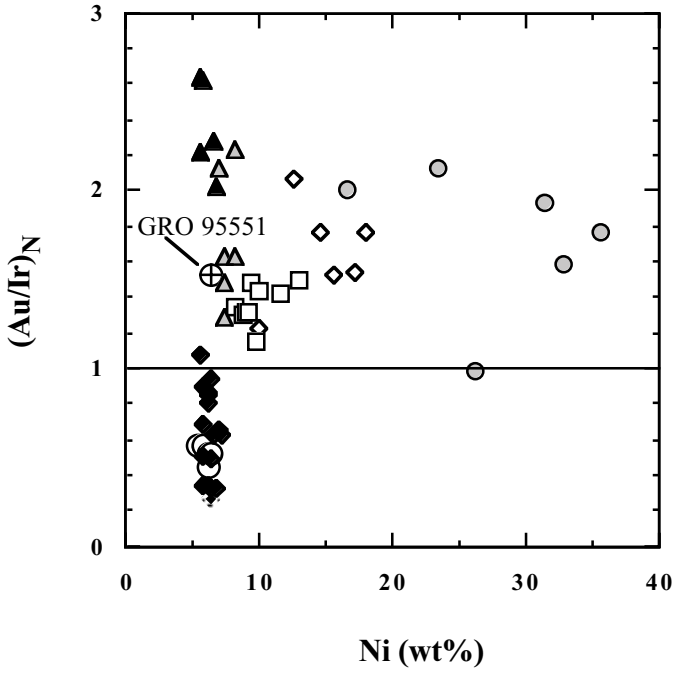

Figure 10

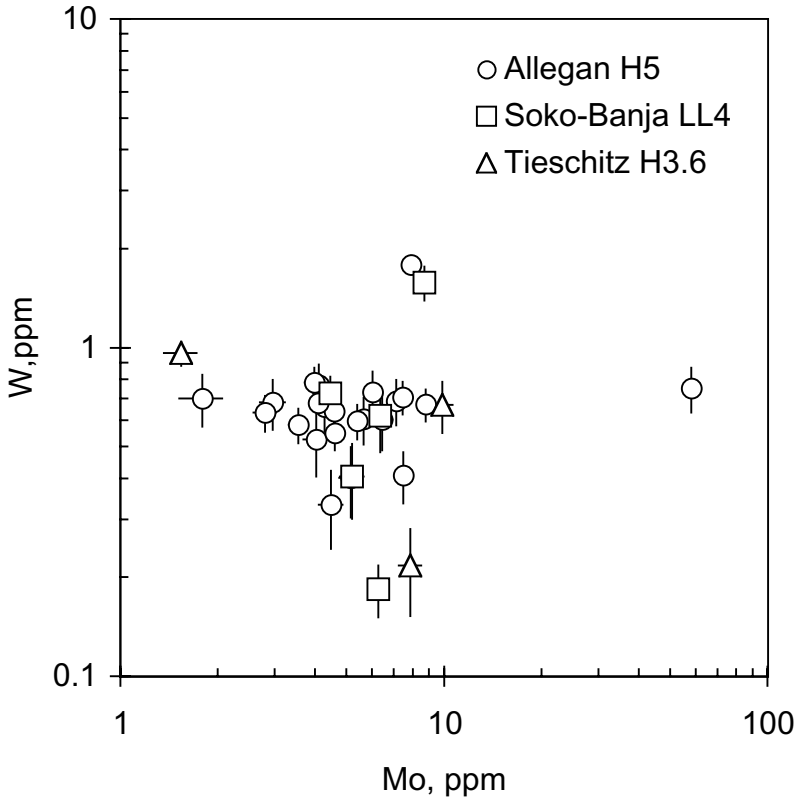
10
1
0.1
W,ppm
1
10
100
Mo, ppm
Allegan H5
Soko-Banja LL4
Tieschitz H3.6

Figure 11